American Mineralogist, Volume 91, pages 894–906, 2006

Heat capacities and entropies of mixing of pyrope-grossular ($Mg_3Al_2Si_3O_{12}$-$Ca_3Al_2Si_3O_{12}$) garnet solid solutions: A low-temperature calorimetric and a thermodynamic investigation

EDGAR DACHS[1,*] AND CHARLES A. GEIGER[2]

[1]Fachbereich Materialwissenschaften, Universität Salzburg, Hellbrunnerstrasse 34, A-5020 Salzburg, Austria
[2]Institut für Geowissenschaften, Abteilung Mineralogie, Christian-Albrechts-Universität Kiel, Olshausenstr. 40,D-24098 Kiel, Germany

ABSTRACT

The low-temperature heat capacities for a series of synthetic garnets along the pyrope-grossular (Py-Gr) join were measured with the heat capacity option of the Physical Properties Measurement System (PPMS) produced by Quantum Design. The measurements were performed between 5 and 300 K on milligram-sized polycrystalline garnets that have been well characterized in previous studies. The C_P measurements indicate positive excess heat capacities (ΔC_P^{xs}) for all solid-solution compositions at temperatures <50 K with a maximum value of 2.31 ± 0.18 J/(mol·K) for the composition $Py_{50}Gr_{50}$ at about 35 K. Pyrope-rich garnets (i.e., $Py_{90}Gr_{10}$ and $Py_{75}Gr_{25}$) have no or slightly positive ΔC_P^{xs} at higher temperatures, whereas grossular-rich garnets (i.e., $Py_{10}Gr_{90}$ and $Py_{25}Gr_{75}$) show negative ΔC_P^{xs} values in the temperature range between 50 and 150 K. At $T > 150$ K, ΔC_P^{xs} values scatter around zero for all compositions and the experimental error is too large to permit a clear determination of whether ΔC_P^{xs} is different from zero within 2σ uncertainty. Excess entropies (ΔS^{xs}) at 298.15 K, calculated from the C_P data of the various solid-solution members, are asymmetric in nature with the largest positive deviations in pyrope-rich compositions. An asymmetric Margules mixing model was found to be inappropriate for modeling the ΔS^{xs}-X data and, thus, a two-parameter Redlich-Kister model was used to describe the excess entropy-composition relationships. Using this macroscopic mixing model for the excess entropy, a T-X diagram for Py-Gr garnets was calculated using different published values for the excess enthalpies of mixing. The effect of short range Ca-Mg order in the solid solution also was considered in the calculations. The calculations give a solvus for the pyrope-grossular join with a higher critical temperature in the range 850–1330 °C at $X_{Gr} = 0.35$ compared to previous thermodynamic models ($T_{crit} < 600$ °C) that use symmetric mixing models to describe the excess entropy. Unmixing of garnets in nature, as documented from occurrences in ultramafic diatremes may, therefore, have occurred at higher temperatures than previously thought. The atomistic and lattice-dynamic properties of Py-Gr garnets are reviewed and compared to the macroscopic C_P data. Published IR and Raman spectra are consistent with the occurrence of positive ΔC_P^{xs} values at low temperatures.

Keywords: Calorimetry, pyrope-grossular garnet solid solutions, thermodynamics, excess heat capacities, excess entropies

INTRODUCTION

The determination of thermodynamic properties of minerals plays a central role in the fields of mineralogy, petrology, and geochemistry. Indeed, after many years of work there exists, today, good data for the different thermodynamic functions for most end-member oxides and silicates (e.g., Robie and Hemingway 1995; Berman 1988; Holland and Powell 1998). It is a fact, however, that most rock-forming silicates are solid solutions and thus it is imperative to determine their mixing properties to understand their thermodynamic behavior. However, although much effort has been undertaken in this regard, truly quantitative thermodynamic mixing properties for many rock-forming silicate and oxide solid solutions are still not available (Geiger 2001a). This lack of data hinders thermodynamic calculations for many problems in the Earth Sciences and, therefore, much work needs to be done in this area.

Heat capacity (C_P) is a fundamental thermodynamic property and it is measured using various calorimetric methods (see for example, Gmelin 1987 or Cezairliyan 1988, for a review). Unfortunately, there is a dearth of heat-capacity measurements on mineral solid solutions and, thus, their entropies of mixing are poorly known (Geiger 2001b). Through C_P, the vibrational part of the third-law entropy (S_0) of a substance at 298.15 K can be determined via (e.g., Ulbrich and Waldbaum 1976):

$$S_0 = \int_0^{298.15} \frac{C_P}{T} dT + \Delta S_{trans} + S_r = S_{298.15}^{cal} + S_r \quad (1)$$

where ΔS_{trans} is any entropy change resulting from a phase transition between 0 and 298.15 K, and S_r is the residual entropy incorporating all quenchable contributions such as frozen-in structural disorder (often referred to as configurational entropy). The C_P integral in Equation 1 is generally the most important contribution to the entropy and it is accessible by calorimetric

* E-mail: edgar.dachs@sbg.ac.at

techniques and (combined with ΔS_{trans},) may be termed the calorimetric entropy $S^{cal}_{298.15}$.

Until recently, low-temperature heat capacities mainly have been determined by adiabatic or quasi-adiabatic calorimetry. This method has the advantage of being very precise, but has the experimental disadvantage of requiring at least several grams of material for measurement (Gmelin 1987). This explains the lack of C_P data for many systems of mineralogical, petrological, and geophysical importance. In the two binary silicate solid-solution systems, pyrope-grossular, $(Mg,Ca)_3Al_2Si_3O_{12}$, and analbite-sanidine, $(Na,K)AlSi_3O_8$, where the C_P of mixing has been measured, it has been shown that large positive excess heat capacities are present at temperatures below 200 K for intermediate compositions (Haselton and Westrum 1980; Haselton et al. 1983). In the case of garnet of composition $Py_{60}Gr_{40}$, it was proposed that the excess C_P can be as much as 25% around 40 K. At temperatures between 300 and 1000 K, the pyrope-grossular binary shows no excess heat capacity as determined by differential scanning calorimetry (DSC) measurements (Bosenick et al. 1996). Moreover, the IR spectra of various binary aluminosilicate garnet solid solutions can be interpreted as indicating that low-temperature excess heat capacities of mixing should be present for pyrope-grossular solid solutions (Geiger 1998). Thus, these studies demonstrate the urgent need for further low-temperature heat-capacity measurements on garnet solid solutions.

In this paper, we present low-temperature heat-capacity measurements between 5 and 300 K on synthetic pyrope-grossular garnets using low-temperature heat-pulse calorimetry. This relatively new method (for the field of mineralogy, see Dachs and Bertoldi 2005) allows for the measurement of samples weighing milligrams. As a result of this technological advancement, we are able to extend the important calorimetric study of Haselton and Westrum (1980) on pyrope-grossular solid solutions. This binary has received much study both in terms of theory and experiment and is relatively well understood in terms of its crystal-chemical, lattice-dynamic, and macroscopic thermodynamic properties (for a review, see Geiger 1999, 2004; Bosenick et al. 2000, 2001; Vinograd et al. 2004 and references therein). It can be argued that pyrope-grossular garnets, because of the number of investigations made on them, serve as a "cutting-edge" system for investigating the physical nature of solid-solution behavior. Our C_P measurements offer the possibility to investigate, once again, the thermodynamic mixing behavior of an important silicate solid solution from a microscopic to macroscopic level.

Experimental methods

Synthesis and characterization of pyrope-grossular garnets

The samples that were investigated by low-T heat-pulse calorimetry come from two sources. The first set of garnets used for measurement is that studied by Haselton and Westrum (1980), and it includes the two end-members pyrope (Py), $Mg_3Al_2Si_3O_{12}$, and grossular (Gr), $Ca_3Al_2Si_3O_{12}$, and one solid-solution composition $Py_{60}Gr_{40}$. A description of the synthesis conditions and the characterization of the garnets can be found in their original publication. As stated in Haselton and Westrum (1980), impurities in their garnets occurred in very small amounts (<1%) and electron microprobe analysis showed that the garnet compositions are similar to their nominal compositions. Thus, we used in our calculations of excess properties the nominal compositions of the garnet (i.e., $X_{Gr} = 0.00$, 0.40, and 1.00, where X_{Gr} is the mole fraction of the grossular component, which in the case of the garnets studied equals the site fraction X_{Ca} in the garnet structure).

The second set of pyrope-grossular garnets, used in this study, was synthesized by C.A. Geiger. Most of these garnets have been exceptionally well characterized both chemically and structurally using a variety of diffraction, spectroscopic, and calorimetric methods. The garnets studied in this work have the following nominal compositions: Py, $Py_{90}Gr_{10}$, $Py_{75}Gr_{25}$, $Py_{60}Gr_{40}$, $Py_{50}Gr_{50}$, $Py_{25}Gr_{75}$, and $Py_{10}Gr_{90}$. A description of the synthesis conditions and the characterization for most of the compositions can be found in Bosenick et al. (1995, 1999), Geiger (1998), Kolesov and Geiger (1998), Boffa Ballaran et al. (1999), and Dapiaggi et al. (2005). The garnets Py, $Py_{90}Gr_{10}$, $Py_{75}Gr_{25}$, $Py_{50}Gr_{50}$, and $Py_{25}Gr_{75}$ are the exact same samples used in the DSC study of Bosenick et al. (1996). Based on microprobe data given in Bosenick et al. (1995, 1996), the composition of the garnets in terms of X_{Gr} for Py, $Py_{90}Gr_{10}$, $Py_{75}Gr_{25}$, $Py_{60}Gr_{40}$, $Py_{50}Gr_{50}$, $Py_{25}Gr_{75}$, and $Py_{10}Gr_{90}$ is: X_{Gr} = {0.00, 0.104, 0.264, 0.414, 0.512, 0.76, 0.904}. The grossular studied by Bosenick et al. (1996) was not used for PPMS measurement.

Low-temperature calorimetry using a physical properties measurement system

Low-temperature heat capacities were measured with a commercially designed calorimeter [heat capacity option of the Physical Properties Measurement System (PPMS), constructed by Quantum Design], which has been set up at Salzburg University. The measurements were performed at temperatures between 5 and 300 K on synthetic polycrystalline garnets weighing between 17 and 26 mg and contained in hermetically sealed Al containers. C_P data were collected at 50 different temperatures on cooling from 300 K with a logarithmic spacing, with C_P measured three times at each temperature (see Appendix[1]). Details of the experimental method (heat-pulse calorimetry: HPC, e.g., Hwang et al. 1997), as well as the data acquisition and evaluation procedures, including a discussion of data precision and accuracy for mineralogical samples, are given in Dachs and Bertoldi (2005). Therefore, they will only be discussed briefly here.

The central part of the PPMS calorimeter is the so-called calorimeter puck that resides at the base of a sample chamber. This, in turn, forms the inner part of a probe that is immersed directly in a liquid helium bath contained within a larger liquid-nitrogen-jacketed dewar. The calorimeter puck consists of the puck frame and the sample platform that holds the sample. The puck is covered with a cap (i.e., thermal radiation shield). The sample holder is a 4×4 mm wide sapphire platform that has a thermometer and a heater attached to the lower side. This sample platform has thin Pt wires attached to it that complete the electrical connection and provide for structural support between the platform and the puck frame.

In HPC, as technically constructed in the PPMS calorimeter, a known amount of heat is introduced to a sample at user-defined set points of T and the resulting temperature response is measured. To determine heat capacity quantitatively, two separate measurements, an "*addenda run*" and a "*sample run*" are necessary. For an *addenda run*, the heat capacity of the empty sample platform, including some grease to achieve thermal contact with the sample to be studied, is determined using a differential equation based on Fourier's law of heat conduction and the law of conservation of energy ("one-τ model"). The relevant equation is:

$$C_P^{pl} \frac{dT_{pl}(t)}{dt} = P_{in}(t) - K_W \left[T_{pl}(t) - T_b \right] \quad (2)$$

where "pl" stands for platform, $dT_{pl}(t)/dt$ is the thermal response of the sample platform to which a square-pulse of heat $P_{in}(t)$ is applied, K_w is the thermal conductance of the Pt wires (in units of W/K), and T_b the temperature of the puck frame. A nonlinear least-squares fit to the analytical solutions of Equation 2 (Eqs. 6a and 6b of Dachs and Bertoldi 2005) yields the heat capacity of the empty sample platform, C_P^{pl}, at the temperature T_{pl}. This procedure is then repeated at the desired temperature with the sample mounted on the sample platform ("*sample run*"). The thermal model in this case requires an additional term to Equation 2 that accounts for the heat flow between the sample and the sample platform and is given by:

[1] Deposit item AM-05-021, Appendix. Deposit items are available two ways: For a paper copy contact the Business Office of the Mineralogical Society of America (see inside front cover of recent issue) for price information. For an electronic copy visit the MSA web site at http://www.minsocam.org, go to the American Mineralogist Contents, find the table of contents for the specific volume/issue wanted, and then click on the deposit link there.

$$C_P^{pl}\frac{dT_{pl}(t)}{dt} = P_{in}(t) - K_W\left[T_{pl}(t) - T_b\right] - K_g\left[T_{pl}(t) - T_s(t)\right] \quad (3a)$$

where K_g is the thermal conductance of the grease located between the sample and sample platform and T_s is the temperature of the sample. The temperature change in the sample with respect to time, dT_s/dt, its heat capacity, C_P^s, and the heat flow to or from it are governed by the relationship:

$$C_P^s\frac{dT_s(t)}{dt} = K_g\left[T_{pl}(t) - T_s(t)\right] \quad (3b)$$

Because the PPMS calorimeter measures the temperature of the platform, T_{pl}, T_s is eliminated by inserting Equation 3a into 3b, yielding:

$$\frac{d^2T_{pl}}{dt^2} + \frac{dT_{pl}}{dt}\left[\frac{(C_P^sK_w / K_g + C_P^s + C_P^{pl})K_g}{C_P^sC_P^{pl}}\right] + \frac{K_wK_g}{C_P^sC_P^{pl}}T_{pl} = \frac{K_g}{C_P^sC_P^{pl}}\left[P(t) + K_wT_b\right] \quad (4)$$

Because the heat capacity of the platform plus grease is already known from the "*addenda run*", there remain four unknowns: K_g, K_w, T_b, and C_P^s. Based on the temperature-time response curve measured during the sample run (40–200 data pairs for each measurement at a given temperature), these unknowns are solved for by applying the same non-linear least-squares fitting routine to the analytical solution of Equation 4 as used previously to calculate the addenda heat capacity. The standard deviation of each measurement, σ_{C_P}, can be obtained from this fitting procedure. The heat capacity contribution of the Al-container is evaluated and subtracted from the total heat capacity to give the net heat capacity of the unknown sample (Dachs and Bertoldi 2005).

Dachs and Bertoldi (2005) showed by comparing C_P values measured on powders of standard reference materials SRM-720 (corundum), sanidine, and fayalite using the PPMS to C_P values measured by low-temperature adiabatic calorimetry (low-*T* AC) that the former C_P values tend to be systematically lower by 1–2% than those measured by low-*T* AC in the temperature range between 100 and 300 K. At low *T*, where the absolute values of C_P are small, PPMS-C_P values may be up to 50% larger than those measured by low-*T* AC. It was also shown that entropies derived from PPMS C_P measurements are at most 1–2% lower than entropies calculated from low-*T* AC experiments. These "systematic errors" (assuming that the low-*T* AC technique measures the "true value"), however, will cancel out, if excess heat capacities and entropies for a binary solid solution, for example, are considered.

Data evaluation

The first step in the data evaluation is to convert from units of [μJ/K] to molar units [J/(mol·K)]. One has C_P in J/(mol·K) = C_P in μJ/K × 10^{-3} × (formula weight)/(sample weight). An uncertainty of ±0.02 mg for the sample weight has been applied for this calculation (for details see Dachs and Bertoldi 2005).

The resulting molar C_P data (see Appendix) were then fitted to a C_P-polynomial of the general form $C_P = k_o + k_1T^{-0.5} + k_2T^{-2} + k_3T^{-3} + k_4T + k_5T^2 + k_6T^3$ using the function "LinearFit" of the Experimental Data Analyst Package of Mathematica. For this purpose, the data set was divided into three temperature regions, whereby each was fit individually, but such that a certain overlap of data was present (i.e., the polynominal $C_P = k_o + k_1T^{-0.5} + k_2T^{-2} + k_3T^{-3}$ was used for fitting the high-*T* portion of the data, and the complete polynomial given above for the interval 5–35 K, and $C_P = k_2T^{-2} + k_4T + k_5T^2 + k_6T^3$ for the C_P data for the interval 35–130 K). This procedure resulted in a good description of the experimental data (i.e., deviation usually <0.3%). The C_P values below 5 K were estimated from a plot of C_P/T vs. T^2 and a linear extrapolation to 0 K (i.e., $C_P = k_6T^3$). The resulting C_P coefficients and the temperatures for the various "data" intervals are given in Table 1.

The calorimetric entropies at 298.15 K, $S^{cal}_{298.15}$, of the pyrope-grossular solid solutions were then determined by solving stepwise analytically the C_P integral in Equation 1. The uncertainty in $S^{cal}_{298.15}$ was determined in the following two ways and they yielded identical results. The two calculation procedures are:

(1) If a total of *n* C_P-*T* data pairs have been measured (where *n* = 150 for this study), the integral in Equation 1 can be approximated numerically by:

$$S^{cal}_{298.15} = \sum_{i=0}^{n-1}\frac{\hat{\tau}_i + \delta_i + \hat{\tau}_{i+1} + \delta_{i+1}}{2}\Delta T_i \quad (5)$$

where $\tau_i = C_{Pi}/T_i$, ΔT_i is the temperature difference between successive measurements, and each τ_i is regarded as consisting of the unknown true value, $\hat{\tau}_i$, with an error δ_i. Thus, one has $\tau_i = \hat{\tau}_i + \delta_i$. Rearranging Equation 5 yields:

$$S^{cal}_{298.15} \cong \sum_{i=0}^{n-1}\frac{\hat{\tau}_i + \hat{\tau}_{i+1}}{2}\Delta T_i + \sum_{i=0}^{n-1}\frac{\delta_i + \delta_{i+1}}{2}\Delta T_i \quad (6)$$

The second term in Equation 6 is necessary for deriving the standard deviation of $S^{cal}_{298.15}$ from σ_{Cpi} and can be written in terms of the variances, S, of discrete random variables, Θ_i, for each C_P measurement, for which δ_i is one possible value:

$$\sigma^2(S^{cal}_{298.15}) = S(S^{cal}_{298.15}) = S\left(\sum_{i=0}^{n-1}\frac{\Theta_i + \Theta_{i+1}}{2}\Delta T_i\right) \quad (7)$$

Equation 7 is valid, if the errors associated with each C_P measurement are distributed normally and are independent of each other. Applying the rules for variances yields:

$$\sigma^2(S^{cal}_{298.15}) = \frac{1}{4}\left(\Delta T_0^2S(\Theta_0) + (\Delta T_0 + \Delta T_1)^2S(\Theta_1) + (\Delta T_1 + \Delta T_2)^2S(\Theta_2) + \ldots + (\Delta T_{n-2} + \Delta T_{n-1})^2S(\Theta_{n-1}) + \Delta T_{n-1}^2S(\Theta_n)\right) \quad (8)$$

The variances, $S(\Theta_i)$, in Equation 8 are calculated by error propagation from the C_P measurements as:

$$S(\Theta_i) = \sigma^2\left(C_{P_i}/T_i\right) = \left(1/T_i\right)^2\sigma^2_{Cp_i} \quad (9)$$

The temperature uncertainty in the PPMS C_P measurements is about one order of magnitude less than σ_{CP} and has been neglected in Equation 9.

(2) A Monte-Carlo technique is applied to the measured C_P data and their standard deviations using the Mathematica functions "RandomArray" and "NormalDistribution" to calculate a randomly distributed error for each measurement. In this way, a set of artificial C_P data was created and integrated to get $S^{cal}_{298.15}$. This procedure was repeated *n* times and the mean and standard deviation of these data give $S^{cal}_{298.15}$ and $\sigma_{Scal,298.15}$. It was found that $\sigma_{Scal,298.15}$ derived by this Monte-Carlo method converges to $\sigma_{Scal,298.15}$, as calculated above under procedure 1, if $n \geq 1000$. Note that, because errors in C_P tend to cancel out in the integration, the relative uncertainty $\sigma_{Scal,298.15}/S^{cal}_{298.15}$ is smaller than σ_{C_P}/C_P and is usually around 0.1%.

Results

C_P and S_0 of pyrope and grossular

The C_P measurements on the two garnet end-members, pyrope and grossular, are shown in Figures 1a and 1b, and they are in reasonable to good agreement with the data of Haselton and Westrum (1980). At low *T*, the heat capacity of grossular is less than that of pyrope (Fig. 1a), whereas at ambient *T* the situation is the reverse (Fig. 1b). The C_P crossover occurs at around 170 K. Compared to the C_P data of Haselton and Westrum (1980), most of the PPMS data are 1–2% lower at $T > 100$ K and somewhat higher at $T < 100$ K (Fig. 2). A similar behavior was observed previously for PPMS measurements made on powders of corundum (SRM-720), fayalite, and sanidine vs. their values determined by low-*T* AC (Dachs and Bertoldi 2005).

The various C_P values at 298.15 K are compared in Table 2 with those from the literature. The standard third-law entropies, S_0, are also given in Table 2, and they are in excellent agreement with literature data [the Py–3 has with –0.7% the largest deviation, whereas that for Gr–1 is 0.9% lower than S_0 according to Haselton and Westrum (1980); the agreement of the other measurements is better].

Excess heat capacities and entropies of mixing of pyrope-grossular solid solutions

Excess heat capacities of mixing, ΔC_P^{xs}, were calculated according to the equation

$$\Delta C_P^{xs} = C_P^{ss} - [(1 - X_{Gr})\,C_P^{Py} + X_{Gr}\,C_P^{Gr}] \quad (10)$$

TABLE 1. Coefficients for the C_p polynomial $C_p = k_o + k_1T^{-0.5} + k_2T^{-2} + k_3T^{-3} + k_4T + k_5T^2 + k_6T^3$

PPMS run	Py-1	Py-2	Py-3	Py-4	$Py_{90}Gr_{10}$-1	$Py_{90}Gr_{10}$-2	$Py_{90}Gr_{10}$-3	$Py_{75}Gr_{25}$-1
Source	HW80	HW80	Geiger	Geiger	Geiger	Geiger	Geiger	Geiger
FW	403.129	403.129	403.129	403.129	407.955	407.955	407.955	415.716
SW	23.74	23.74	27.17	27.17	22.44	22.44	16.75	21.22
X_{Gr}	0.000	0.000	0.000	0.000	0.102	0.102	0.102	0.264
k_6	8.7622E–05	9.5293E–05	9.5140E–05	1.4172E–04	9.5416E–05	1.0448E–04	8.2806E–05	7.7958E–05
T_1	4.94	6.32	8.35	5.07	6.20	5.92	5.90	5.32
k_o	6.1266E+00	–6.7024E+00	–1.0340E+01	–3.9297E+00	–4.9740E+00	–8.5034E+00	–6.1028E+00	1.1268E+01
k_1	–1.5085E+01	1.5712E+01	2.4072E+01	8.3704E+00	1.2578E+01	2.0655E+01	1.5356E+01	–2.5158E+01
k_2	6.3672E+01	–7.0451E+01	–1.0298E+02	–3.0553E+01	–6.9046E+01	–9.8811E+01	–8.0987E+01	8.7591E+01
k_3	–1.1189E+02	1.3764E+02	1.9511E+02	5.5310E+01	1.4813E+02	1.9658E+02	1.6863E+02	–1.4400E+02
k_4	–2.2049E–01	3.4151E–01	5.1740E–01	2.4893E–01	2.3134E–01	4.0001E–01	2.7519E–01	–5.4746E–01
k_5	2.2090E–03	–1.4139E–02	–1.9856E–02	–1.2339E–02	–1.0461E–02	–1.5670E–02	–1.1412E–02	1.4647E–02
k_6	2.1026E–04	4.0184E–04	4.6839E–04	3.8403E–04	3.6882E–04	4.3264E–04	3.7626E–04	6.4288E–05
T_2	38.26	34.85	32.84	22.55	33.85	33.26	34.96	33.62
k_2	–1.0482E+03	6.2965E+02	8.2777E+02	1.0684E+03	7.8604E+02	8.4687E+02	6.3521E+02	3.2515E+02
k_4	–3.5115E–01	–4.4361E–01	–4.5651E–01	–4.6609E–01	–4.2969E–01	–4.3664E–01	–4.1830E–01	–3.5309E–01
k_5	1.9031E–02	2.1107E–02	2.1038E–02	2.1125E–02	2.0832E–02	2.1029E–02	2.0677E–02	1.9034E–02
k_6	–6.0787E–05	–7.2071E–05	–7.1352E–05	–7.0893E–05	–7.0376E–05	–7.1295E–05	–6.9870E–05	–6.1431E–05
T_3	147.69	126.80	129.05	109.83	128.88	128.98	130.99	134.22
k_o	7.3447E+02	7.7157E+02	7.4371E+02	7.7987E+02	7.6703E+02	7.6835E+02	7.4054E+02	7.2527E+02
k_1	–7.1571E+03	–7.9359E+03	–7.2737E+03	–8.1262E+03	–7.8176E+03	–7.8255E+03	–7.2761E+03	–6.8377E+03
k_2	–3.2434E+05	7.2453E+05	–4.4699E+05	1.1073E+06	6.9570E+05	6.6248E+05	4.9575E+03	–1.0184E+06
k_3	1.1825E+08	4.9626E+07	1.3231E+08	1.7931E+07	4.2263E+07	4.6081E+07	8.5178E+07	1.6549E+08
T_4	298.15	298.15	298.15	298.15	260.11	263.80	257.97	274.50
k_o					5.7403E+02	5.7038E+02	5.7196E+02	5.8285E+02
k_1					–2.2742E+03	–2.1395E+03	–2.2028E+03	–2.3619E+03
k_2					–1.7174E+07	–1.8075E+07	–1.7515E+07	–1.8511E+07
k_3					2.0381E+09	2.1966E+09	2.0763E+09	2.3254E+09
T_{max}					1200.00	1200.00	1200.00	1200.00
$C_p^{298.15}$	320.8	322.0	322.4	322.4	326.0	326.0	325.7	325.6
$S^{cal}_{298.15}$	265.94	265.81	264.20	265.01	268.09	268.65	268.06	267.48

Notes: Coefficients for the C_p polynomial $C_p = k_o + k_1T^{-0.5} + k_2T^{-2} + k_3T^{-3} + k_4T + k_5T^2 + k_6T^3$ derived by fitting the PPMS C_p data of pyrope-grossular garnets given in the Appendix [T in K, C_p in J/(mol·K)]. At the bottom of the table, heat capacity and entropy at 298.15 K are additionally given in J/(mol·K). Different parts of the C_p polynomial apply in different temperature intervals, defined by temperatures T_1 up to T_4. At these temperatures, fits yield identical C_p. The PPMS data for some compositions ($Py_{90}Gr_{10}$, $Py_{75}Gr_{25}$, $Py_{50}Gr_{50}$, $Py_{25}Gr_{75}$) have been combined with the DSC data of Bosenick et al. (1996) above 320 K and a further set of C_p coefficients is given for those allowing calculation of C_p up to T_{max}.
Source of samples measured is either Haselton and Westrum (1980, HW80), or garnets synthesized by C.A. Geiger.
FW = Formula weight [g/mol]; SW = sample weight [mg].

TABLE 1. —*Continued*

PPMS run	$Py_{60}Gr_{40}$-1	$Py_{60}Gr_{40}$-2	$Py_{50}Gr_{50}$-1	$Py_{25}Gr_{75}$-1	$Py_{10}Gr_{90}$-1	$Py_{10}Gr_{90}$-2	Gr-1	Gr-2
Source	HW80	Geiger	Geiger	Geiger	Geiger	Geiger	HW80	HW80
FW	422.059	422.059	427.358	439.094	445.722	445.722	450.452	450.452
SW	24.05	21.91	23.22	21.02	25.01	25.01	25.81	25.81
X_{Gr}	0.400	0.414	0.512	0.760	0.904	0.904	1.000	1.000
k_6	6.9651E–05	9.9837E–05	1.0331E–04	1.8543E–04	2.2054E–04	1.8920E–04	1.0233E–04	6.9161E–05
T_1	5.88	6.41	6.06	6.23	6.45	5.43	7.24	5.95
k_o	7.7404E+00	4.5351E+00	8.9892E–01	–2.3943E+01	–1.7803E+01	–1.8336E+01	–1.0069E+01	–1.0677E+01
k_1	–1.3437E+01	–5.7324E+00	3.3294E+00	5.8291E+01	4.1048E+01	4.2092E+01	2.4437E+01	2.5841E+01
k_2	6.8000E+00	–2.7401E+01	–6.3766E+01	–2.5660E+02	–1.6450E+02	–1.6532E+02	–1.1368E+02	–1.1777E+02
k_3	3.2167E+01	9.6852E+01	1.5626E+02	4.7853E+02	2.9918E+02	2.9538E+02	2.2369E+02	2.2693E+02
k_4	–5.5529E–01	–4.1281E–01	–3.0127E–01	9.6461E–01	8.4074E–01	8.7111E–01	4.4631E–01	4.7118E–01
k_5	2.1478E–02	1.7278E–02	1.7728E–02	–2.1210E–02	–2.3783E–02	–2.4727E–02	–1.4218E–02	–1.4807E–02
k_6	–8.3552E–05	–3.5213E–05	–8.7353E–05	3.3141E–04	3.9309E–04	4.0393E–04	3.1578E–04	3.2120E–04
T_2	25.41	26.78	31.47	30.72	30.46	30.93	29.05	36.48
k_2	5.6647E+02	6.3091E+02	1.0051E+03	2.1973E+03	2.7398E+03	2.8266E+03	2.1899E+03	2.1806E+03
k_4	–3.0896E–01	–3.1509E–01	–3.1002E–01	–4.0096E–01	–4.9496E–01	–5.0022E–01	–5.1079E–01	–5.1611E–01
k_5	1.7537E–02	1.7624E–02	1.7293E–02	1.8079E–02	1.9225E–02	1.9360E–02	1.9878E–02	2.0130E–02
k_6	–5.3395E–05	–5.3468E–05	–5.1303E–05	–5.2771E–05	–5.6402E–05	–5.7262E–05	–6.0534E–05	–6.1905E–05
T_3	124.01	123.56	144.86	154.05	124.35	124.96	126.45	122.52
k_o	7.7636E+02	8.0952E+02	7.5273E+02	7.4573E+02	7.9397E+02	7.7818E+02	7.9318E+02	7.4905E+02
k_1	–7.9116E+03	–8.6563E+03	–7.4598E+03	–7.1977E+03	–8.1559E+03	–7.8285E+03	–8.2725E+03	–7.2456E+03
k_2	3.5384E+05	1.5533E+06	–4.0585E+04	–7.5903E+05	3.9494E+05	–6.6162E+04	8.3929E+05	–7.6160E+05
k_3	7.7572E+07	–6.0548E+06	9.4485E+07	1.4844E+08	7.5630E+07	1.0657E+08	4.2462E+07	1.4992E+08
T_4	298.15	298.15	255.68	263.00	298.15	298.15	298.15	298.15
k_o			5.9772E+02	5.5952E+02				
k_1			–2.9429E+03	–1.4371E+03				
k_2			–1.4797E+07	–2.2276E+07				
k_3			1.7367E+09	2.7333E+09				
T_{max}			1200.00	1200.00				
$C_p^{298.15}$	325.1	325.5	326.4	328.8	328.9	328.1	325.1	326.5
$S^{cal}_{298.15}$	265.11	265.44	265.480	262.44	259.58	259.23	257.86	259.47

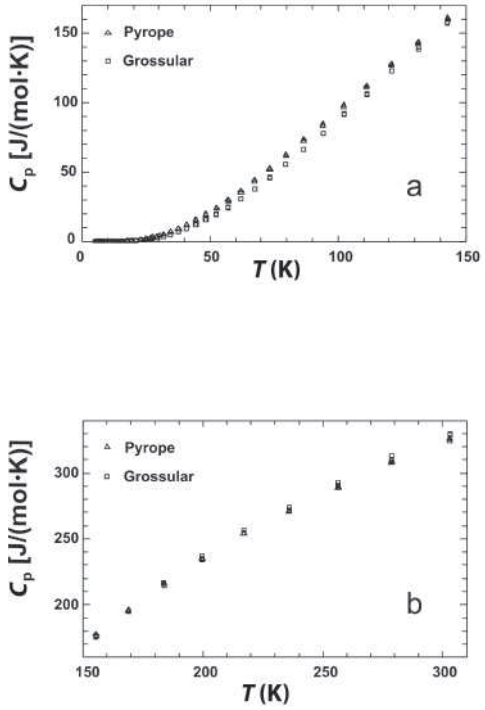

FIGURE 1. Heat capacity of pyrope and grossular in the temperature range 5–150 K (**a**) and 150–300 K (**b**). Data are given in the Appendix (all pyrope and grossular PPMS measurements).

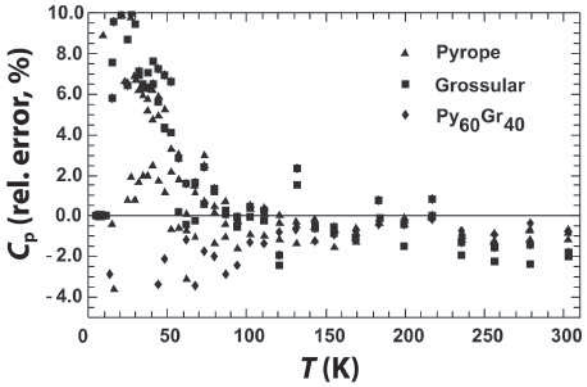

FIGURE 2. Relative errors in % {= 100 × [C_P(PPMS) – C_P(low-T AC)]/[C_P(low-T AC)]} for the heat capacities of pyrope, grossular and the solid solution $Py_{60}Gr_{40}$ compared to the C_P data of Haselton and Westrum (1980) measured using low-temperature adiabatic calorimetry (low-T AC).

using the fitted C_P polynomials for the various garnet solid solutions and end-members (the fit to the C_P data of PY–1 was used for pyrope and the fit of Gr–2 for grossular). The uncertainty in ΔC_P^{xs} was determined by applying an error propagation to Equation 10 that included the uncertainty σ_{C_P} of the PPMS measurement and an assumed uncertainty in garnet composition of ±0.01. The values of ΔC_P^{xs} as functions of composition at different temperatures are shown in Figures 3a–3d. Figures 4a and

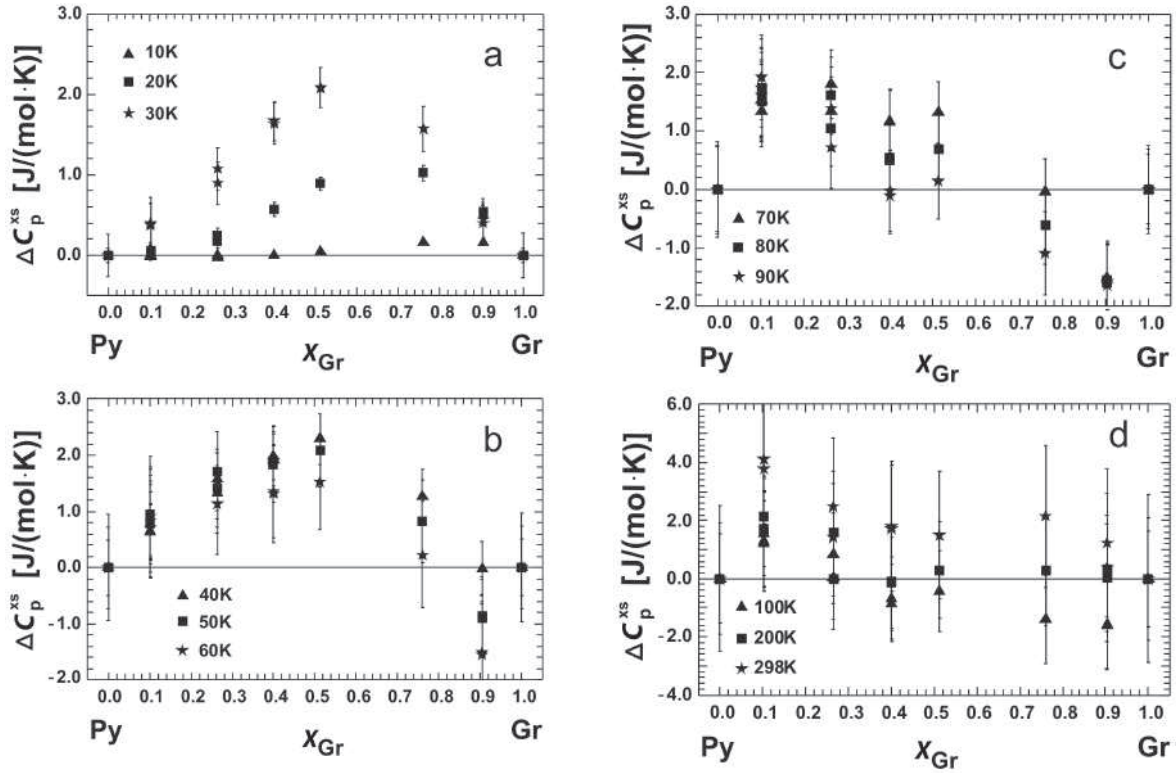

FIGURE 3. Excess heat capacities of pyrope-grossular garnets as function of composition (X_{Gr}) at various temperatures. Error bars are 2σ.

TABLE 2. C_p values at 298.15 K and standard third-law entropies S_o of pyrope and grossular

Garnet	PPMS Run	C_p^{PPMS} J/(mol·K)	C_p^{HW80} J/(mol·K)	C_p^{B96} J/(mol·K)	S_o^{PPMS} J/(mol·K)	S_o^{HW80} J/(mol·K)	S_o^{B88} J/(mol·K)	S_o^{HP98} J/(mol·K)	S_o^{G97} J/(mol·K)
Pyrope	Py-1*	320.8±0.9	325.31	325.5	265.94±0.23	266.27	266.36	266.3	274.45±0.27‡
	Py-2*	322.0±0.8			265.81±0.22				
	Py-3†	322.4±0.9			264.20±0.23				
	Py-4†	322.4±1.0			265.01±0.24				
Grossular	Gr-1*	325.1±1.0	333.17	331.3	257.86±0.26	260.12	255.15	255	257.47±0.24
	Gr-2*	326.5±1.0			259.47±0.25				

Notes: Sample and formula weights are given in Table 1. HW80: Haselton and Westrum (1980); B96: Bosenick et al. (1996); B88: Berman (1988); HP98: Holland and Powell (1998); G97: Gottschalk (1997).

* Same sample as studied by Haselton and Westrum (1980).

† Same sample as studied by Bosenick et al. (1996).

‡ Based on the low-T C_p measurements of Kolesnik et al. (1977) on a natural pyrope-rich garnet with 18.8 mol% almandine and 8.2 mol% grossular component.

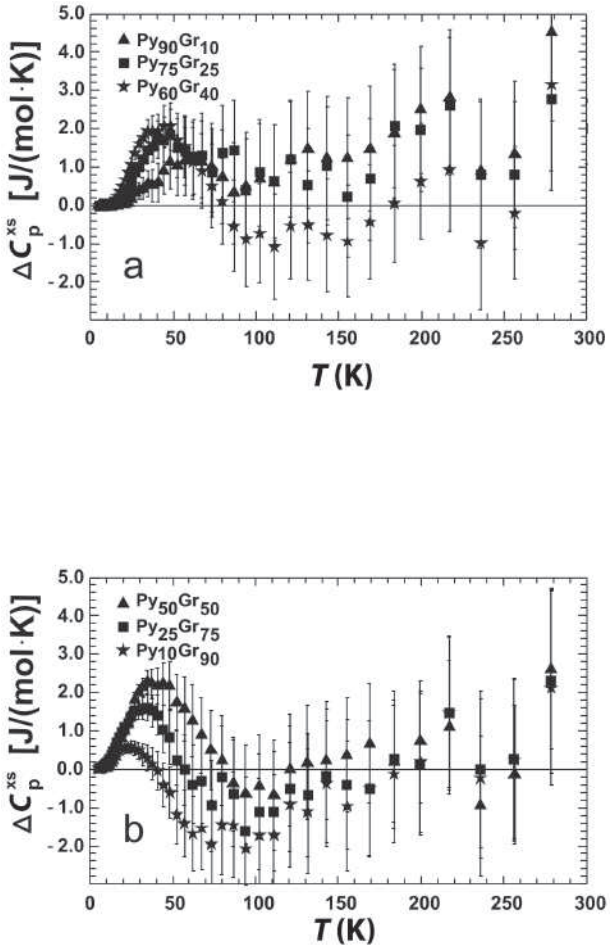

FIGURE 4. Excess heat capacities of pyrope-grossular garnets as function of temperature for (**a**) the solid-solution members $Py_{90}Gr_{10}$, $Py_{75}Gr_{25}$, and $Py_{60}Gr_{40}$, and (**b**) $Py_{50}Gr_{50}$, $Py_{25}Gr_{75}$, and $Py_{10}Gr_{90}$. Error bars are 2σ. The data of PPMS-run $Py_{60}Gr_{40}$ (sample 1 from Haselton and Westrum 1980) are shown. The data for Py60Gr40 (sample 2 from C.A. Geiger) yield very similar values and are not shown.

4b display the ΔC_P^{xs} values for the various Py-Gr solid solutions as functions of temperature.

It can be observed that positive ΔC_P^{xs} start to develop at grossular-rich compositions at 10 K (Fig. 3a) and increase in magnitude with increasing T. Concurrently, the maximum in ΔC_P^{xs} shifts toward the compositionally intermediate part of the join and reaches a maximum value of 2.31 ± 0.18 J/(mol·K) for the composition $Py_{50}Gr_{50}$ at about 35 K (Figs. 3a and 4b). The composition $Py_{60}Gr_{40}$ shows a smaller positive ΔC_P^{xs} of 2.00 ± 0.17 J/(mol·K) at about 35 K. This result may be compared to the value of $\Delta C_P^{xs} = 3.4$ J/(mol·K) as determined by Haselton and Westrum (1980) for the same composition around $T = 40$ K. As can be observed in Figure 4, positive ΔC_P^{xs} values are present for all solid-solution compositions at low temperatures.

It also can be observed that the experimental errors increase continuously with increasing temperature (Fig. 4). The ΔC_P^{xs} data indicate that pyrope-rich garnets (i.e., $Py_{90}Gr_{10}$ and $Py_{75}Gr_{25}$) have no or slightly positive ΔC_P^{xs} at the higher temperatures. Grossular-rich garnets ($Py_{10}Gr_{90}$ and $Py_{25}Gr_{75}$—Fig. 4b) show, on the other hand, a region of slightly negative ΔC_P^{xs} values, outside the limits of experimental error, in the temperature range between 50 and 150 K. At $T > 150$ K, ΔC_P^{xs} values scatter around zero and the experimental error is too large to determine if ΔC_P^{xs} is significantly different from zero within 2σ uncertainty (the reason for the decrease in the C_P values around 250 K is not clear).

The excess entropies for the Py-Gr join at 298.15 K can be calculated via the relation:

$$\Delta S^{xs} = S^{cal}_{298.15} - [(1 - X_{Gr})\, S_0^{Py} + X_{Gr}\, S_0^{Gr}] \quad (11)$$

The resulting values are listed in Table 3. As shown by DSC measurements (Bosenick et al. 1996) on pyrope-grossular garnets, ΔC_P^{xs} is zero above 320 K and thus ΔS^{xs} and ΔH^{xs} are temperature independent at these higher temperatures. To make calculations of ΔS^{xs}, S_0 of PPMS measurement PY–1 was used for pyrope and S_0 of PPMS measurement Gr–2 for grossular (Table 3; Model 1), because they yielded values of S_0 similar to those reported by Haselton and Westrum (1980). Another model fit using the slightly lower S_0 value for grossular based on PPMS measurement Gr–1 is discussed below (Model 2). The uncertainty in ΔS^{xs} was calculated in a manner similar to that described above for ΔC_P^{xs}.

The results show the following: The grossular-rich garnet $Gr_{90}Py_{10}$ has approximately zero or even a slightly negative ΔS^{xs} value (Fig. 5). This arises because the positive ΔC_P^{xs} values around 40 K are "compensated" for (or even "overcompensated") by negative ΔC_P^{xs} values at higher temperatures (Fig. 4b). The other Gr-rich garnet $Gr_{75}Py_{25}$ has a positive ΔS^{xs} value. With increasing pyrope content in garnet, the ΔS^{xs} values generally tend to increase and show a value of ~3.3 ± 0.3 J/(mol·K) for the composition $Gr_{25}Py_{75}$. The two ΔS^{xs} values from the PPMS

TABLE 3. Calorimetric entropies at 298.15 K ($S^{cal}_{298.15}$) for solid-solution members of the pyrope-grossular join and excess entropies (ΔS^{xs}) derived according to Equation 11

Garnet	PPMS Run	Composition X_{Gr}	$S^{cal}_{298.15}$ J/(mol K)	Model 1 ΔS^{xs} J/(mol K)	Model 1 $\Delta S^{xs}/(1-X_{Gr})X_{Gr}$	Model 2 ΔS^{xs} J/(mol K)	Model 2 $\Delta S^{xs}/(1-X_{Gr})X_{Gr}$
Py	Py-1*	0.000	265.94±0.23	0.00±0.33		0±0.34	
$Py_{90}Gr_{10}$	$Py_{90}Gr_{10}$-1†	0.102	268.09±0.22	2.81±0.31	30.7±3.4	2.97±0.31	32.5±3.4
	$Py_{90}Gr_{10}$-2†	0.102	268.65±0.21	3.37±0.30	36.8±3.3	3.53±0.31	38.6±3.3
	$Py_{90}Gr_{10}$-3†	0.102	268.06±0.27	2.78±0.35	30.4±3.8	2.94±0.35	32.1±3.8
$Py_{75}Gr_{25}$	$Py_{75}Gr_{25}$-1†	0.264	267.48±0.24	3.25±0.31	16.7±1.6	3.67±0.31	18.9±1.6
$Py_{60}Gr_{40}$	$Py_{60}Gr_{40}$-1*	0.400	265.11±0.22	1.76±0.29	7.3±1.2	2.40±0.29	10.0±1.2
	$Py_{60}Gr_{40}$-2†	0.414	265.44±0.24	2.18±0.30	9.0±1.2	2.85±0.31	11.7±1.3
	HW80*‡	0.400	268.32	4.50±0.30	18.8±1.3	4.50±0.30	18.8±1.3
$Py_{50}Gr_{50}$	$Py_{50}Gr_{50}$-1†	0.512	265.48±0.23	2.85±0.29	11.4±1.2	3.68±0.30	14.7±1.2
$Py_{25}Gr_{75}$	$Py_{25}Gr_{75}$-1†	0.760	262.44±0.25	1.42±0.33	7.8±1.8	2.64±0.33	14.5±1.8
$Py_{10}Gr_{90}$	$Py_{10}Gr_{90}$-1†	0.904	259.58±0.23	-0.51±0.33	-5.9±3.8	0.94±0.33	10.9±3.8
	$Py_{10}Gr_{90}$-2†	0.904	259.23±0.22	-0.86±0.32	-9.9±3.7	0.59±0.33	6.8±3.8
Gr	Gr-2*	1.000	259.47±0.25	0.00±0.36			
	Gr-1*	1.000	257.86±0.26			0±0.36	

Notes: The datum of HW80 for $Py_{60}Gr_{40}$ is included for comparison. Model 1 uses S_o of grossular from PPMS-run Gr-2, model 2 from PPMS-run Gr-1 to calculate excess properties, S_o of pyrope is identical in both models. Sample sources:
* Same samples as studied by Haselton and Westrum (1980).
† Same samples as studied by Bosenick et al. (1996).
‡ Original result of Haselton and Westrum (1980) on $Py_{60}Gr_{40}$.

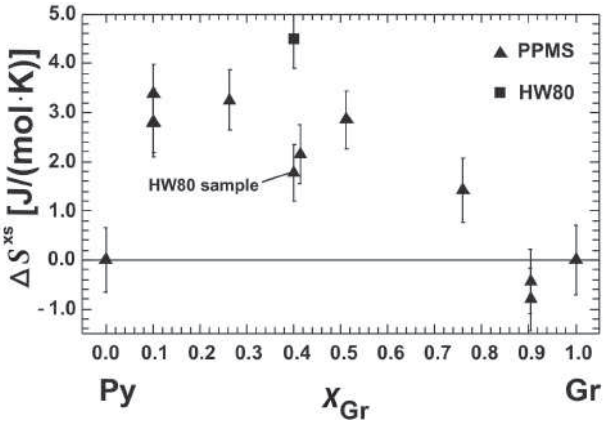

FIGURE 5. Excess entropies, ΔS^{xs}, of pyrope-grossular garnets as function of composition (X_{Gr}) at 298.15 K. Data are from Table 3 (Model 1). Note the asymmetric behavior with a maximum ΔS^{xs} at pyrope-rich compositions. Error bars are 2σ. The datum of HW80 is shown for comparison.

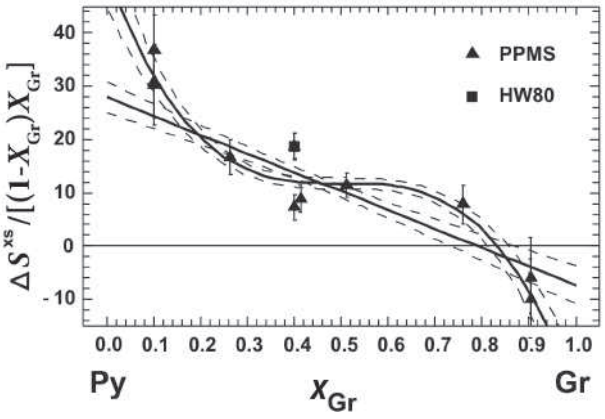

FIGURE 6. Plot of $\Delta S^{xs}/[(1-X_{Gr})X_{Gr}]$ vs. X_{Gr} (data from Table 3; Model 1) showing two mixing models. The two-parameter Redlich-Kister model is given by the curve and the two-parameter Margules formalism by the straight line. The dashed lines represent 2σ-uncertainties.

measurements for the composition $Py_{60}Gr_{40}$, including a remeasurement of the original sample of Haselton and Westrum (1980), are somewhat lower, both with $\Delta S^{xs} \sim 2.0 \pm 0.3$ J/(mol·K). A notable experimental result is the substantial positive ΔS^{xs} of 3.1 ± 0.3 J/(mol·K) for the composition $Py_{90}Gr_{10}$. To ensure the correctness of this result, three separate PPMS measurements were performed on this sample and all three yielded similar C_P (i.e., ΔS^{xs}) values. C_P measurements on $Py_{10}Gr_{90}$ and $Py_{60}Gr_{40}$ were also repeated and confirm the $S^{cal}_{298.15}$ and ΔS^{xs} values (Table 3). In conclusion, the C_P data show that the Py-Gr join is characterized by an asymmetry in its ΔS^{xs} behavior.

THERMODYNAMIC MODELING

Margules and Redlich-Kister description of the ΔS^{xs}-X_{Gr} data

The ΔS^{xs} data can be modeled in several ways (Ganguly 2001). If a subregular Margules mixing model of the type:

$$\Delta S^{xs} = (1 - X_{Gr})X_{Gr}\,[W_{S,GrPy} + (W_{S,PyGr} - W_{S,GrPy})X_{Gr}] \quad (12)$$

is taken to model the data, a plot of $\Delta S^{xs}/(1-X_{Gr})X_{Gr}$ vs. X_{Gr} should yield a straight line with the intercept $W_{S,GrPy}$ and a slope given by $(W_{S,PyGr} - W_{S,GrPy})$. Figure 6 shows the relevant data (see also Table 3; Model 1). Asymmetric ΔS^{xs} behavior for the Py-Gr join is confirmed by such an analysis. Using the Mathematica function "LinearFit," the Margules entropy parameters $W_{S,PyGr} = -7.4 \pm 3.4$ J/(pfu K) and $W_{S,GrPy} = 27.9 \pm 1.4$ J/(pfu K) are obtained (pfu = per formula unit). These values are compared with estimates from the literature in Table 4. We note, however, that the positive ΔS^{xs} value for $Py_{90}Gr_{10}$, and also that ΔS^{xs} for $Py_{25}Gr_{75}$ are not well described by a two-parameter Margules model.

A better description of the ΔS^{xs}-X_{Gr} data can be made by use of a two-parameter Redlich-Kister solution model of the form:

$$\Delta S^{xs} = (1 - X_{Gr})X_{Gr}\,[A_0 + A_3(1 - 2X_{Gr})^3] \quad (13)$$

TABLE 4. Redlich-Kister parameters (A_o, A_3) and Margules entropy-parameters ($W_{S,PyGr}$, $W_{S,GrPy}$) derived in this study for modeling excess entropy of the pyrope-grossular join and compared to literature data [three cation mixing, units J/(pfu K)]

Mixing model	Redlich-Kister		Margules	
Parameter	A_o	A_3	$W_{S,PyGr}$	$W_{S,GrPy}$
Model 1	11.8 ± 0.5	39.7 ± 3.2	–7.4 ± 3.4	27.9 ± 1.4
Model 2	15.1 ± 0.5	27.2 ± 3.1	3.8 ± 3.4	24.8 ± 1.5
BA96			18.79	18.79
G96			17.34 (11.01)*	17.34 (11.01)*
M97			2.49 ± 5.16	20.82 ± 3.23

Notes: Model 1 and 2 values differ only in the value for S_o that is taken for end-member grossular and used to calculate ΔS^{xs} (see text for further details). Parameters were derived using the ΔS^{xs} errors given in Table 3 and assuming an error of 0.01 in X_{Gr}.
BA96 = Berman and Aranovich (1996), G96 = Ganguly et al. (1996), M97 = Mukhopadhyay et al. (1997).
* 11.01 is the optimized and 17.34 is the preferred value (Ganguly et al. 1996).

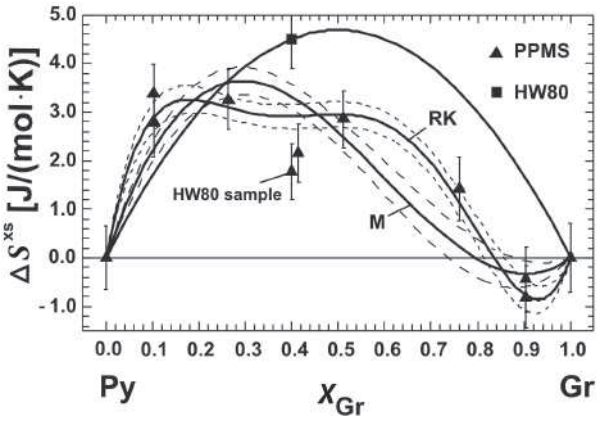

FIGURE 7. Two-parameter Redlich-Kister (curve labeled RK) and two-parameter Margules (curve labeled M) description of the excess entropy along the join pyrope-grossular. The experimental data (Table 3; Model 1) are shown. The dashed lines are 2σ-uncertainty curves. The symmetric curve is ΔS^{xs} according to Haselton and Newton (1980) calculated with W_s = 18.79 J/(pfu K).

A model fit using this equation yields A_o = 11.8 ± 0.5 J/(pfu K) and A_3 = 39.7 ± 3.2 J/(pfu K) for three-cation mixing (Table 4; Model 1). The resulting model fit is shown in Figure 6.

Figure 7 compares both the two-parameter Margules and the two-parameter Redlich-Kister models. It appears that the Redlich-Kister model provides a more appropriate description for the excess entropies for the Py-Gr system. A symmetric mixing model is also shown in Figure 7. It is that of Haselton and Newton (1980) and is based on the single Haselton and Westrum (1980) C_P datum for the garnet $Py_{60}Gr_{40}$. The resulting interaction parameter from a one parameter Margules model is W_s = 18.79 J/(pfu K) as used, for example, in the data set of Berman and Aranovich (1996).

Activity-composition relationships and unmixing behavior

There have been several studies made to model the activity-composition relationships of pyrope-grossular garnets (e.g., Hensen et al. 1975; Haselton and Newton 1980; Ganguly et al. 1996; Vinograd 2001; Vinograd et al. 2004). The data herein allow a further attempt to obtain a quantitative description of the thermodynamic behavior of this solid solution. We present calculations in which the activity coefficients at 1 bar were calculated with the equations:

$$RT\ln\gamma_{Py} = \Delta H^{xs} - X_{Gr}\left(\frac{\partial \Delta H^{xs}}{\partial X_{Gr}}\right) - T\left[\Delta S^{xs} - X_{Gr}\left(\frac{\partial \Delta S^{xs}}{\partial X_{Gr}}\right)\right] \quad (14a)$$

and

$$RT\ln\gamma_{Gr} = \Delta H^{xs} + (1-X_{Gr})\left(\frac{\partial \Delta H^{xs}}{\partial X_{Gr}}\right) - T\left[\Delta S^{xs} + (1-X_{Gr})\left(\frac{\partial \Delta S^{xs}}{\partial X_{Gr}}\right)\right] \quad (14b),$$

which result from decomposing ΔG^{xs} into respective excess enthalpy and entropy terms. The pressure effect on the activity coefficients was calculated from the relationship:

$$RT\ln\gamma_i^{P,T} = RT\ln\gamma_i^{1,T} + \Delta v^{xs}_i(P-1) \quad (15)$$

where Δv^{xs}_i is the partial molar excess volume of mixing of component i, which was calculated from the Margules volume parameters $W_{V,PyGr}$ = 0.184 and $W_{V,GrPy}$ = 0.012 J/bar for three cation mixing (Bosenick and Geiger 1997).

In deriving pyrope and grossular activities from Equations 14 and 15 at P and T, we use

$$\Delta H^{xs} = (1-X_{Gr})X_{Gr}\,[W_{H,GrPy} + (W_{H,PyGr} - W_{H,GrPy})X_{Gr}] \quad (16)$$

with the Margules enthalpy parameters $W_{H,PyGr}$ = 29502 and $W_{H,GrPy}$ = 64881 J/pfu as taken from Ganguly et al. (1996).

The excess entropy was calculated using either the preferred Redlich-Kister model or the asymmetric Margules model with the parameters cited above (Model 1). The resulting activity-composition diagrams are shown in Figures 8a and 8b for P = 1 bar for temperatures from 400 to 1300 °C (one-cation mixing). An important aspect of both diagrams is the nature of the activity curves, which indicate that two different garnet compositions can have identical activities. Thus, unmixing along the Py-Gr binary should occur. It is also apparent that using the Redlich-Kister model for ΔS^{xs} (Fig. 8a), unmixing will occur at higher temperatures compared to the case with the Margules description of the ΔS^{xs} data (Fig. 8b). In Figure 9, we show binary solvi, using the Redlich-Kister model for ΔS^{xs}, calculated from the relationships:

$$a_{Py}^{Grt1} = a_{Py}^{Grt2} \quad (17a)$$

and

$$a_{Gr}^{Grt1} = a_{Gr}^{Grt2} \quad (17b)$$

Both conditions must be fulfilled at thermodynamic equilibrium to have coexisting Py-rich and Gr-rich garnets, given here as Grt1 and Grt2. The critical temperature for the solvus calculated from activities using the Model 1 parameters for ΔS^{xs} is 1247 °C

TABLE 5. Critical temperatures (°C) of the solvi along the pyrope-grossular binary calculated using ΔS^{xs}_{vib} of this study (either Model 1 or 2 parameters of the Redlich-Kister and Margules descriptions from Table 4) and combined with various ΔH^{xs} from the literature

ΔH^{xs}	ΔS^{xs}: This study Redlich-Kister		ΔS^{xs}: This study Margules	
According to:	Model 1	Model 2	Model 1	Model 2
Ganguly et al. (1996)	1247	927	523	529
Berman and Aranovich (1996)	1327	991	577	575
Newton et al. (1977)	853	614	335	326

Notes: The solvi based on the prefered Redlich-Kister model for ΔS^{xs}_{vib} are shown in Figure 9 and have their critical temperatures at X_{Gr} = 0.35–0.4. The Margules based solvi have a temperature maximum at the composition X_{Gr} = 0.44–0.49 for Model 1 parameters and at X_{Gr} = 0.36–0.39 for Model 2 parameters and are broader.

(1 bar) (labeled M1-G in Fig. 9). It is considerably higher than the critical temperature (around 520 °C) for the corresponding solvus obtained from a Margules mixing model (critical temperatures of the Margules-based solvi are given in Table 5, but not plotted in Fig. 9). The solid points shown in this figure are the synthesis temperatures for the Py-Gr solid solutions used in this study (Bosenick et al. 1996).

DISCUSSION

Model results and mixing behavior

As noted above, we have used the standard entropy values of S_0 = 265.94 J/(mol·K) for pyrope (PPMS-run PY–1) and S_0 = 259.47 J/(mol·K) for grossular (PPMS-run Gr–2) in calculating excess entropies for the pyrope-grossular solid solutions. From Table 2 it can be seen that our PPMS-derived S_0 value for pyrope is in excellent agreement with that measured by Haselton and Westrum (1980). Moreover, the S_0 value for pyrope is in good agreement with those taken from various internally consistent thermodynamic databases with the exception of Gottschalk (1997), which relies on the C_P data of Kolesnik et al. (1977) measured on a natural pyrope-rich garnet. The excellent agreement concerning the S_0 value of pyrope confirms its use in the calculations made above.

For the case of grossular, however, it is known (Geiger 1999) that there is some disagreement regarding its standard entropy value. The various values in the literature range between 255.0 and 260.12 J/(mol·K) (Table 2). If we use S_0 = 257.86 J/(mol·K) for grossular, the value resulting from PPMS-run Gr–1, the magnitudes of the excess heat capacities increase slightly, for example, at 50 K from 1.95 to 2.05 J/(mol·K) for the composition X_{Gr} = 0.512. As a consequence, the excess entropies also increase slightly and ΔS^{xs} behavior is positive for all compositions including the more grossular-rich garnets. A fit based on Model 2 data yields the Redlich-Kister parameters A_o = 15.1 ± 0.5 J/(pfu K) and A_3 = 27.2 ± 3.1 J/(pfu K), and gives the Margules entropy parameters $W_{S,PyGr}$ = 3.8 ± 3.4 J/(pfu K) and $W_{S,GrPy}$ = 24.8 ± 1.5 J/(pfu K) (Table 4; Model 2). As the case with Model 1, a two-parameter Margules model does not describe well the ΔS^{xs} values for the compositions $Py_{90}Gr_{10}$ and $Py_{25}Gr_{75}$. The resulting *T-X* diagram using this Model 2 (Fig. 9, labeled M2-G), yields a solvus with a critical temperature of 927 °C (1 bar) at X_{Gr} = 0.35. Note the difference with the solvus calculated using Model 1.

At this point, we would like to stress that the solvus calculated with either Model 1 or 2 for ΔS^{xs} is dependent on how the data fitting is done. If, for instance, we had included a linear and quadratic term in the Redlich-Kister expression (Eq. 13), the critical temperature according to Model 1 would be 110 °C higher (1345 °C). The parameters A_1 and A_2 are not, however, statistically significant and the simpler two-parameter description is preferred.

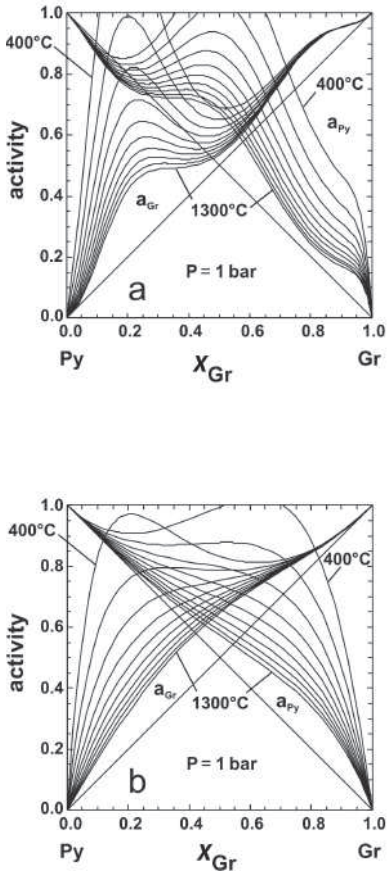

FIGURE 8. Activities for pyrope and grossular components in pyrope-grossular solid solutions at temperatures from 400 to 1300 °C and P = 1 bar using (**a**) the Redlich-Kister model and (**b**) the Margules model for ΔS^{xs} of this study (one cation mixing). Enthalpic interaction parameters of $W_{H,PyGr}$ = 29502 and $W_{H,GrPy}$ = 64881 J/pfu are from Ganguly et al. (1996).

We also adopted different values for ΔH^{xs} to explore their effect on pyrope-grossular phase relations. If we accept the Margules enthalpy parameters of Berman and Aranovich (1996), that is $W_{H,PyGr}$ = 33470 and $W_{H,GrPy}$ = 68280 J/(pfu), the critical temperature of the 1-bar solvus calculated according to Model 1 for ΔS^{xs} is 1327 °C and for Model 2 is 991 °C (solvi labeled M1-BA and M2-BA in Fig. 9). The temperature maxima of these solvi correspond to the composition X_{Gr} = 0.37. If, on the other hand, we use ΔH^{xs} taken from Newton et al. (1977), that is $W_{H,PyGr}$ = 25104 and $W_{H,GrPy}$ = 47949 J/(pfu), the critical temperature of the 1-bar solvus according to Model 1 is 853 °C and for Model 2 is 614 °C (solvi labeled M1-N and M2-N in Fig. 9).

It should be noted further that any contributions of S_{conf}, which are related to Mg-Ca order-disorder in the solid solutions

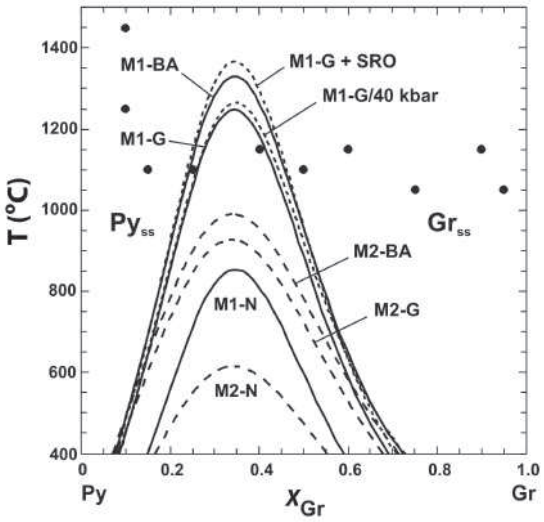

FIGURE 9. *T-X* phase diagram for the pyrope-grossular binary based on the Redlich-Kister model for ΔS_{vib}^{xs} of this study. Calculations with Model 1 parameters for $\Delta S_{vib}{}^{xs}$ (Table 4) are labeled M1 (solid curves) and those with Model 2 parameters M2 (dashed curves). They have been combined with ΔH^{xs} values of Ganguly et al. (1996; labeled G), Berman and Aranovich (1996; labeled BA), or Newton et al. (1977; labeled N). All solvi have been computed for P = 1 bar, with the exception of the dashed curve labeled M1-G/40 kbar, for which P = 40 kbar. The dashed solvus labeled M1-G + SRO includes the maximal effect of short range order. The solid points represent the synthesis temperatures for the garnets used in this study. Critical temperatures for the various solvi are given in Table 5.

(Bosenick et al. 1995, 1999, 2000; Vinograd 2001; Vinograd et al. 2004), have been neglected in calculating activities. If the distribution of Mg and Ca in solid-solution compositions is not completely random, a configurational entropy contribution to the total excess entropy arises, in addition to the excess vibrational entropy ΔS_{vib}^{xs} (=ΔS^{xs} used previously). This additional term is a measure of the difference between the configurational entropy of a real solution compared to one with a random distribution of Ca and Mg cations (and thus a maximal S_{conf}):

$$\Delta S^{xs} = \Delta S_{vib}^{xs} + (S_{conf}^{real} - S_{conf}^{random}) \quad (18)$$

Based on ^{29}Si NMR spectroscopic measurements and static lattice-energy calculations, Bosenick et al. (1995, 1999, 2000) proposed that a small degree of Ca-Mg short-range order (SRO) is present in intermediate pyrope-grossular garnets with X_{Gr} = 0.15–0.75. Thus, S_{conf}^{real} is smaller than in the case of random mixing and, consequently, the difference of $S_{conf}^{real} - S_{conf}^{random}$ is negative with a maximum at X_{Gr} = 0.5. Vinograd (2001) and Vinograd et al. (2004) calculated using the cluster-variation method S_{conf}^{real} and obtained values between ~4.5 and 5.5 J/(mol·K) for intermediate compositions and temperatures between 400 and 1400 °C (Vinograd 2001). Bosenick et al. (2000) undertook static lattice-energy calculations, combined with Monte Carlo techniques, and computed similar values of S_{conf}^{real} for the Py-Gr solid solution. The configurational entropy corresponding to the case of complete random mixing of Ca and Mg is 5.763 J/(mol·K) for X_{Gr} = 0.5 for one cation mixing using the relationship $S_{conf}^{random} = -R \Sigma X_i \ln X_i$.

To further explore the effect of SRO on pyrope-grossular phase relations, we assume a value of S_{conf}^{real} = 5 J/(mol·K) at X_{Gr} = 0.5 that is temperature independent. This is a reasonable first-order approximation and should be valid at temperatures around 600 °C (Vinograd 2001). Thus, a maximum value of ($S_{conf}^{real} - S_{conf}^{random}$) = –0.763 J/(mol·K) can be taken for intermediate compositions. The compositional dependence can be described by a symmetric Margules mixing model:

$$S_{conf}^{real} - S_{conf}^{random} = (1 - X_{Gr}) X_{Gr} W_{S,SRO} \quad (19)$$

with $W_{S,SRO}$ = –3.052 J/(mol·K).

If this value is taken to describe the SRO and then used in Equations 14a and 14b, the critical temperature for a solvus based on Model 1 for ΔS_{vib}^{xs} increases by ~120 to ~1350 °C (Fig. 9—labeled M1-G + SRO). This is the maximum effect that SRO will have on unmixing behavior, because the configurational entropy of a real solution approaches that with random mixing at high temperatures. Thus, the difference $S_{conf}^{real} - S_{conf}^{random}$ tends to zero, which is not taken into account in our first-order model calculation.

Summarizing, the pyrope-grossular binary appears to represent a solid solution where ΔS_{vib}^{xs} cannot be adequately described by an asymmetric Margules model. Instead, a Redlich-Kister model is more appropriate for describing the thermodynamic mixing properties along this join. In terms of the phase relations, previous calculations, based on asymmetric Margules models and using previous C_P data (Ganguly et al. 1996; Wang et al. 2000), predict unmixing to occur at temperatures less than 620 °C. In contrast, based on the present measurements and using a Redlich-Kister model to describe ΔS_{vib}^{xs}, a solvus is obtained that has a much higher critical temperature of up to ~1300 °C for compositions around X_{Gr} = 0.35–0.40.

Petrological implications

Our new calorimetric results have implications for and applications in various petrological problems. For example, Wang et al. (2000) described coexisting garnets of different composition in the system pyrope-almandine-grossular in a pyrope-rich single crystal collected from an ultramafic diatreme at Garnet Ridge, Arizona. They interpreted the host-inclusion texture to represent an immiscible garnet pair, based on the observation that the compositional difference between them increased approaching the common interface. They estimated temperatures of unmixing in the approximate range between 400 and 450 °C using the garnet mixing model presented by Ganguly et al. (1996). These estimated temperatures could be too low and in our opinion temperatures greater than 600 °C may be more correct. If we take the garnet compositions reported by Wang et al. (2000) (i.e., host: ~$Alm_{16}Py_{66}Gr_{17}Sp_1$ and inclusion: ~$Alm_{14}Py_{42}Gr_{43}Sp_1$), and correct for the almandine component of around 15 mol% and the very low spessartine component in both garnets, we obtain renormalized compositions of $Py_{80}Gr_{20}$ for the garnet host and $Py_{49}Gr_{51}$ for the inclusion. According to Figure 9, and using the Model 1 ΔS^{xs} solvus (e.g., M1-G or M1-BA), a temperature of unmixing around 900 °C is indicated. At this temperature, both compositions fall on the solvus limbs. The effect of the almandine component on the phase relations will be to lower this value and

the temperature of unmixing for coexisting ternary garnets could possibly be in the temperature range of 800–900 °C. Of course, further calorimetric studies on other binary garnet solid solutions are urgently needed (Geiger 1999) before more quantitative garnet mixing models can be constructed.

Another application for our results can be made using the grospydite xenoliths from the Zagadochnaya kimberlite pipe in Siberia, Russia (Sobolev et al. 1968). Here, grossular-rich nearly binary Py-Gr garnets show compositions between 0.53 < X_{Gr} < 0.81 (Sobolev et al. 1968). These mantle xenoliths probably equilibrated at high temperatures (~1000 °C?) and the observed compositions are consistent with our phase-diagram for Py-Gr garnets (Fig. 9). Moreover, based on the Redlich-Kister derived ΔS^{xs} solvi of Figure 9, zoned pyrope-grossular garnets, with reported compositions of $Alm_3Py_{35}Gr_{60}Sp_2$ for the core and $Alm_7Py_{48}Gr_{44}Sp_1$ for the rim, found in diamondiferous carbonate-silicate rocks of the Kokchetav Massif, Kazakhstan (Sobolev et al. 2001), should also have formed at high temperatures (>1000 °C). This condition is compatible with their geological occurrence.

Lattice-dynamic properties and microscopic-macroscopic relationships

Citing Kieffer (1985, p. 118) in Reviews in Mineralogy "Microscopic to macroscopic" "… detailed studies of macroscopic thermodynamic properties and of lattice vibrational characteristics should provide rich ground for research for many years."

The various thermodynamic mixing properties (i.e., ΔS^{xs}, ΔH^{xs}, and ΔV^{xs}) for the pyrope-grossular binary are the best determined of the six binaries in the quaternary garnet system pyrope-almandine-grossular-spessartine (Geiger 1999), and with the new results herein, an even better level of description can be obtained. This circumstance permits further investigation (i.e., Geiger 2001b) into the underlying physical nature of mixing properties of the garnets in terms of their crystal-chemical and lattice-dynamic properties. We stress, however, that although 20 years have passed since Kieffer's statement, in terms of mineralogical solid-solution systems, investigations along these lines are still in the beginning stages and must be considered simple in nature. Thus, we approach the problem with some care, recognizing that future investigations may nullify or contradict some of our analysis.

It is possible to calculate C_v (or $C_P = C_v + TV\alpha^2K_T$, where V is the volume, α the thermal expansion coefficient, and the K_T isothermal bulk modulus) from the phonon density of states, $G(\nu)$, of a substance using quantum-based lattice-dynamic models. There are several formulations available, whereby the Einstein and Debye models are the simplest and best known (Born and Huang 1954; Dove 1993). With an emphasis on oxides and silicates, Kieffer (1979, 1985) presented a semi-empirical model to calculate heat capacity from the internal energy [i.e., $C_v = (dU^{vib}/dT)_v$] using IR and Raman phonon spectra as input data and which are taken to represent $G(\nu)$. The model contains several simplifications or approximations (i.e., for the dispersion relations, low-energy mode cut offs, etc.), but it appears to provide reasonable C_v/C_P and S_0 values for many silicates. Electronic and magnetic contributions are not directly considered in the formulation (i.e., pyrope-grossular garnets should be the most simple to model using this approach). Hence, lattice-dynamic models can, together with experimental Raman and IR spectra, provide insight into the microscopic vibrational behavior that affects or controls macroscopic C_P behavior (Geiger and Kolesov 2002). This allows one to consider the C_P ($S^{cal}_{298.15}$) mixing behavior of the Py-Gr join. Without going into details (see Kieffer 1985; Gramaccioli 2002), one can describe the heat capacity by:

$$C_v = k_B \int_0^{\nu_{max}} \left(\frac{\hbar\nu}{k_B T}\right)^2 \frac{\exp\left(\hbar\nu/k_B T\right)}{\left[\exp\left(\hbar\nu/k_B T\right)-1\right]^2} G(\upsilon)d\nu \quad (20)$$

where h is Planck's constant, k_B is Boltzmann's constant, ν is the frequency of a normal mode, and $G(\nu)$ is the density of states. To demonstrate this approach, we applied the Kieffer model and calculated C_P for pyrope, grossular and $Py_{60}Gr_{40}$ as function of temperature using the vibrational model of Hofmeister and Chopelas (1991, their Table 1) for the end-members and powder IR spectroscopic data of Boffa Ballaran et al. (1999) for $Py_{60}Gr_{40}$. This calculation was undertaken to test whether our calculations for ΔS^{xs}_{vib} are reasonable in light of lattice-dynamic behavior. Figure 10 shows the corresponding ΔC^{xs}_P for the $Py_{60}Gr_{40}$ composition derived from the Kieffer-model calculation. The good agreement with the measured ΔC^{xs}_P values at low temperatures was achieved by setting the parameters for $Py_{60}Gr_{40}$ in the vibrational model to those values given in the caption to this figure. Above ambient

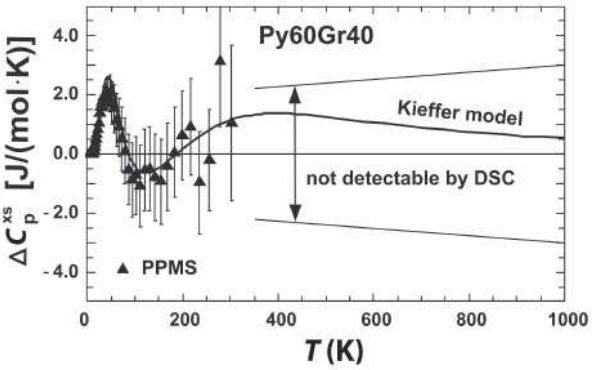

FIGURE 10. Excess heat capacities for $Py_{60}Gr_{40}$ calculated with the Kieffer model (Kieffer 1979) in the temperature range 0–1000 K. For temperatures <300 K, the ΔC_P^{xs} data derived from the PPMS measurements are shown for comparison. Above 300 K the model calculation predicts small positive ΔC^{xs}_P that is below the experimental detection limit of the DSC method (the range shown assumes an optimistic error of only 0.25). The vibrational model of Hofmeister and Chopelas (1991) was used for pyrope and grossular. The input parameters for $Py_{60}Gr_{40}$ were the following (given as pairs: input wave numbers in cm^{-1}, number of modes): Einstein oscillators: (110, 7), (1010, 10), (913, 6), (862, 12), (844, 20), calculated according to Boffa Ballaran et al. (1999, Table 4) for the high frequency oscillators. Treating the lowest energy vibration present in the IR spectra at 110 cm^{-1} as a separate Einstein oscillator (Fig. 7c of Boffa Ballaran et al. 1999) reproduces the experimental positive ΔC^{xs}_P for $Py_{60}Gr_{40}$ around 50 K. Optical continua [given as pairs: wave number range in cm^{-1} (lower to upper cut-off), number of modes]: Continuum 1: (200–355, 26), Continuum 2: (205–263, 36), Continuum 3: (265–476, 24), Continuum 4: (350–402, 36), Continuum 5: (390–557, 24), Continuum 6: (530–653, 36).

conditions, the model calculation predicts positive $\Delta C_P^{xs} < \sim 1.3$ J/(mol·K) that continuously decreases and approaches zero at high temperature. The two thin lines in Figure 10 mark the experimental detection limit given by the DSC technique assuming a limit of 0.25% in C_P. Clearly, the small but nonzero ΔC_P^{xs} given by the model calculation would not be detectable by DSC. Thus, we cannot exclude the possibility that small nonzero ΔC_P^{xs} might be present in the pyrope-grossular solid solution above ambient temperatures. The purely macroscopic-based thermodynamic model for ΔS_{vib}^{xs} presented in this study, which is based on calorimetric measurements, does not account for possible small ΔC_P^{xs} at high temperatures, and thus, treats ΔS_{vib}^{xs} as being temperature independent, at $T > 300$ K.

The C_P measurements of this study confirm the findings of Haselton and Westrum (1980) that the C_P of pyrope is greater than that of grossular at temperatures up to 150 K. The C_P of pyrope is greater, even though it has a smaller unit cell and a lighter mass. This unusual behavior is expressed further in the respective standard entropy values of $S_0 = 265.94 \pm 0.23$ J/(mol·K) for pyrope vs. 257.86 ± 0.26 J/(mol·K) for grossular (Table 2, PPMS-runs Py1, Gr1). This situation has led to discussion in the literature (see for a review Kolesov and Geiger 2000; Geiger 2004). Two crystal-chemical and/or lattice-dynamic explanations have been offered to account for the larger entropy: (1) static spatial disordering of the small Mg cation over subsites in the large dodecahedral cavity or (2) high-amplitude, low-energy vibrations of the Mg cation. Geiger and Kolesov (2002) and Geiger (2004) concluded that the latter explanation (2) best describes the available diffraction and spectroscopic data, although the former explanation (1), which is essentially based on model-dependent lattice-dynamic calculations, can still be found in the literature (e.g., Gramaccioli in Gramaccioli 2002). A key point, here, is that the vibrational behavior of the various dodecahedral **E**-site cations (Geiger 2004) plays an important role in the lattice-dynamic behavior of the aluminosilicate garnets, and thus, further experimental work should be directed to investigating their behavior.

The low-temperature heat capacity is strongly a function of $G(\nu)$ in the low-energy region, which for silicates can depend greatly on the vibrational properties of weakly bonded cations in, for example, large polyhedral sites (i.e., the **E**-site in garnet). This behavior is clearly shown in the phonon density-of-state calculations for pyrope that are based on inelastic neutron scattering measurements (Pavese et al. 1998) and is consistent with the IR and Raman spectra of pyrope (Geiger 1998; Kolesov and Geiger 2000). The question then arises, what is the "microscopic" basis for the macroscopic ΔC_P^{xs} and ΔS^{xs} behavior of pyrope-grossular solid solutions. Two simple explanations have been offered to date. The first calls attention to the lowest energy IR and Raman phonon behavior for those vibrations that have a strong **E**-site character. Here, these lowest energy modes shift to even lower energies for intermediate solid-solution compositions compared to their energies in the end-members pyrope and grossular. This behavior is linked to the positive ΔC_P^{xs} observed at low temperatures, as shown by our calculation with the Kieffer model (Fig. 10). A simple lattice-dynamics explanation is that the small and light Mg cation increases its amplitude of vibration in an "expanded lattice" in solid-solution compositions compared to that in pyrope, thereby lowering its energy of vibration relative to Mg in end-member pyrope (Geiger 1998). This should cause an increase in the heat capacity for the solid solution at low temperatures relative to a mechanical mixture of Py and Gr of the same composition, because it is, once again, the low-energy modes that contribute heavily to C_P at low temperature. Indeed, IR spectra (i.e., Geiger 1998; Bosenick et al. 1999; Boffa Ballaran et al. 1999) indicate that the wavenumber shifts for the lowest energy modes to lower energies is greater in Py-rich compositions compared to Gr-rich compositions. This observation is consistent with the low-temperature ΔC_P^{xs} mixing behavior that shows the greatest positive deviations in Py-rich garnets. The higher energy IR (Geiger 1998; Bosenick et al. 1999; Boffa Ballaran et al. 1999) and Raman modes (Kolesov and Geiger 1998), in contrast, show approximately linear shifts in energy across the Py-Gr binary and are consistent with the ideal heat capacities of mixing that were recorded at temperatures greater than 300 K (Bosenick et al. 1996). The second interpretation considers phonon energy and volume properties (Boffa Ballaran et al. 1999; Rodehorst et al. 2004), whereby nonlinear volume saturation and/or high wavenumber phonon behavior as a function of temperature could be related to excess heat capacities for a solid solution. A weakness in this interpretation lies in the nature of Boltzmann statistics and Equation 20. That is, the population of the high-energy vibrational levels given by, for example, the number of IR and Raman modes located between 800 and 1200 cm^{-1} at low temperatures (i.e., $T < 300$ K) is relatively small and it decreases with decreasing temperature. Therefore, it is difficult to imagine how the temperature saturation behavior of high-energy phonons could account for the large excess heat capacities occurring in Py-Gr solid solutions around 35 K. Of course, we recognize that rigorous lattice-dynamic calculations are needed to test this reasoning. In addition, more complete phonon-density-of-state measurements on intermediate Py-Gr compositions are needed to understand more fully the physical basis of the low temperature C_P data.

ACKNOWLEDGMENTS

We thank H.T. Haselton for generously providing his garnet samples for study. Reviews by M. Gottschalk and an anonymous reviewer helped improve various aspects and we thank them both. This work was financed by the Austrian Science Fund under project number P15880-N11, which is gratefully acknowledged. The research of C.A.G. is supported by the Deutsche Forschungsgemeinschaft — grants Ge 649/14-1 and Ge 649/16-4.

REFERENCES CITED

Berman, R.G. (1988) Internally consistent thermodynamic data for minerals in the system Na_2O-K_2O-CaO-MgO-FeO-Fe_2O_3-Al_2O_3-SiO_2-TiO_2-H_2O-CO_2. Journal of Petrology, 29, 445–522.

Berman, R.G. and Aranovich, L.Ya. (1996) Optimized standard state and solution properties of minerals: I. Model calibration for olivine, orthopyroxene, cordierite, garnet, and ilmenite in the system FeO-MgO-CaO-Al_2O_3-TiO_2-SiO_2. Contributions to Mineralogy and Petrology, 126, 1–24.

Boffa Ballaran, T., Carpenter, M.A., Geiger, C.A., and Koziol, A. (1999) Local structural heterogeneity in garnet solid solutions. Physics and Chemistry of Minerals, 26, 554–569.

Born, M. and Huang, K. (1954) Dynamical theory of crystal lattices. Oxford University Press, London.

Bosenick, A. and Geiger, C.A. (1997) Powder X-ray diffraction study of synthetic pyrope-grossular garnets between 20 and 295 K: A comparison of thermal expansion and heat capacity and volumes of mixing. Journal of Geophysical Research, 102(B10), 22649–22657.

Bosenick, A., Geiger, C.A., Schaller, T., and Sebald, A. (1995) A ^{29}Si MAS NMR and IR spectroscopic investigation of synthetic pyrope-grossular garnet solid solutions. American Mineralogist, 80, 691–704.

Bosenick, A., Geiger, C.A., and Cemic, L. (1996) Heat capacity measurements of

synthetic pyrope-grossular garnets between 320 and 1000 K by differential scanning calorimetry. Geochimica Cosmochimica Acta, 60, 3215–3227.

Bosenick, A., Geiger, C.A., and Phillips, B. (1999) Local Ca-Mg distribution of Mg-rich pyrope-grossular garnets synthesized at different temperatures revealed by ^{29}Si NMR MAS spectroscopy. American Mineralogist, 42, 1422–1433.

Bosenick, A., Dove, M.T., and Geiger, C.A. (2000) Simulation studies on the pyrope-grossular solid solution. Physics and Chemistry of Minerals, 27, 398–418.

Bosenick, A., Dove, M.T., Heine, V., and Geiger, C.A. (2001) Scaling of thermodynamic mixing properties in solid solution minerals. Physics and Chemistry of Minerals, 27, 398–418.

Cezairliyan, A. (1988) Specific Heat of Solids. In C.Y. Ho, Ed., CINDAS Data Series on Material Properties, vol. I–2. Hemisphere Publishing Corporation, New York.

Dachs, E. and Bertoldi, C. (2005) Precision and accuracy of the heat-pulse calorimetric technique: low-temperature heat capacities of milligram-sized synthetic mineral samples. European Journal of Mineralogy, 17, 251–261.

Dapiaggi, M., Geiger, C.A., and Artioli, G. (2005) Microscopic strain in garnet solid solutions determined by synchrotron X-ray diffraction. American Mineralogist, 90, 506–509.

Dove, M.T. (1993) Introduction to lattice dynamics. Cambridge University Press, Cambridge.

Ganguly, J. (2001) Thermodynamic modeling of solid solutions, In C.A. Geiger, Ed., European Notes in Mineralogy—Solid solutions in silicate and oxide systems, 3, p. 71–100.

Ganguly, J., Cheng, W., and O'Neill, H.St.C. (1993) Synthesis, volume, and structural changes of garnets in the pyrope-grossular join: implications for stability and mixing properties. American Mineralogist, 78, 583–593.

Ganguly, J., Cheng, W., and Tirone, M. (1996) Thermodynamics of aluminosilicate garnet solid solution: new experimental data, an optimized model, and thermometric applications. Contributions to Mineralogy and Petrology, 126, 137–151.

Geiger, C.A. (1998) A powder infrared spectroscopic investigation of garnet binaries in the system $Mg_3Al_2Si_3O_{12}$-$Fe_3Al_2Si_3O_{12}$-$Mn_3Al_2Si_3O_{12}$-$Ca_3Al_2Si_3O_{12}$. European Journal of Mineralogy, 3, 407–422.

——— (1999) Thermodynamics of $(Fe^{2+},Mn^{2+},Mg,Ca)_3Al_2Si_3O_{12}$ garnet: An analysis and review. Mineralogy and Petrology, 66, 271–299.

——— Ed. (2001a) Oxide and Silicate Solid Solutions of Geological Importance, 2001, European Mineralogical Union Notes in Mineralogy, v. 3, 465 p. Eötvös University Press, Budapest.

——— (2001b) Thermodynamic mixing properties of binary oxide and silicate solid solutions determined by direct measurements: The role of strain. In C.A. Geiger, Ed., European Notes in Mineralogy—Solid solutions in silicate and oxide systems, 3, p. 71–100.

——— (2004) Spectroscopic investigations relating to the structural, crystal-chemical, and lattice-dynamic properties of $(Fe^{2+},Mn^{2+},Mg,Ca)_3Al_2Si_3O_{12}$ garnet: A review and analysis. In E. Libowitzky and A. Beran, Eds., European Notes in Mineralogy—Spectroscopic Methods in Mineralogy, 6, p. 589–645.

Geiger, C.A. and Kolesov, B.A. (2002) Microscopic-macroscopic relationships in silicates: Examples from IR and Raman spectroscopy and heat capacity measurements. In C.-M. Gramaccioli, Ed., European Notes in Mineralogy—Energy Modelling in Minerals, 4, p. 347–387.

Gmelin, E. (1987) Low-temperature calorimetry: A particular branch of thermal analysis. Thermochimica Acta, 110, 183–208.

Gottschalk, M. (1997) Internally consistent thermodynamic data for rock-forming minerals in the system SiO_2-TiO_2-Al_2O_3-Fe_2O_3-CaO-MgO-FeO-K_2O-Na_2O-H_2O-CO_2. European Journal of Mineralogy, 9, 175–223.

Gramaccioli, C.M., Ed. (2002) Energy Modelling in Minerals. European Notes in Mineralogy, 4, 425 p. Eötvös University Press, Budapest.

Haselton, H.T. and Newton, R.C. (1980) Thermodynamics of pyrope-grossular garnets and their stabilities at high temperatures and high pressures. Journal of Geophysical Research, 85(B12), 6973–6982.

Haselton, H.T., Jr. and Westrum, E.F., Jr. (1980) Low-temperature heat capacities of synthetic pyrope, grossular, and $pyrope_{60}grossular_{40}$. Geochimica Cosmochimica Acta, 44, 701–709.

Haselton, H.T., Jr., Hovis, G.L., Hemingway, B.S., and Robie, R.A. (1983) Calorimetric investigation of the excess entropy of mixing in analbite-sanidine solid solutions: lack of evidence for Na,K short-range order and implications for two-feldspar thermometry. American Mineralogist, 86, 398–413.

Hensen, B.J., Schmid, R., and Wood, B.J. (1975) Activity-composition relationships for pyrope-grossular garnet. Contributions to Mineralogy and Petrology, 51, 161–166.

Hofmeister, A.M. and Chopelas, A. (1991) Thermodynamic properties of pyrope and grossular from vibrational spectroscopy. American Mineralogist, 76, 880–891.

Holland, T.J.B. and Powell, R. (1998) An internally consistent thermodynamic data set for phases of petrological interest. Journal of Metamorphic Geology, 16, 309–343.

Hwang, J.S., Lin, K.J., and Tien, C. (1997) Measurement of heat capacity by fitting the whole temperature response of a heat-pulse calorimeter. Review of Scientific Instruments, 68(1), 94–101.

Kieffer, S.W. (1979) Thermodynamics and lattice vibrations of minerals: 3. Lattice dynamics and an approximation for minerals with application to simple substances and framework silicates. Reviews of Geophysics and Space Physics, 17(1), 35–59.

——— (1985) Heat capacity and entropy: Systematic relations to lattice entropy. In S.W. Kieffer and A. Navrotsky, Eds., Microscopic to macroscopic—Atomic environments to mineral thermodynamics, 14, 65–126. Reviews in Mineralogy, Mineralogical Society of America, Chantilly, Virginia.

Kolesnik, Y.N., Nogteva, V.V., and Paukov, I.Y. (1977) The specific heat of pyrope at 13 to 300 K and the thermodynamic parameters of some natural varieties of garnet. Geochemistry International, 1977, 126–133.

Kolesov, B.A. and Geiger, C.A. (1998) Raman spectra of silicate garnets. Physics and Chemistry of Minerals, 25, 142–151.

——— (2000) Low-temperature single-crystal Raman spectrum of pyrope. Physics and Chemistry of Minerals, 27, 645–649.

Mukhopadhyay, B., Holdaway, M.J., and Koziol, A.M. (1997) A statistical model of the thermodynamic mixing properties of Ca-Mg-Fe^{2+} garnets. American Mineralogist, 82, 165–181.

Newton, R.C., Charlu, T.V., and Kleppa, O.J. (1977) Thermochemistry of high pressure garnets and clinopyroxenes in the system CaO-MgO-Al_2O_3-SiO_2. Geochimica Cosmochimica Acta, 41, 369–377.

Pavese, A., Artioli, G., and Moze, O. (1998) Inelastic neutron scattering from pyrope powder: experimental data and theoretical calculations. European Journal of Mineralogy, 1, 59–70.

Robie, R.A. and Hemingway, B.S. (1995) Thermodynamic properties of minerals and related substances at 298.15 K and 1 bar (10^5 Pascals) pressure and at higher temperatures. United State Geological Survey Bullettin, 2131, 1–431.

Rodehorst, U., Carpenter, M.A., Boffa Ballaran, T., and Geiger, C.A. (2004) Local structural heterogeneity, mixing behaviour and saturation effects in the grossular-spessartine solid solution. Physics and Chemistry of Minerals, 31, 387–404.

Sobolev, N.V., Jr., Kuznetsova, I.K., and Zyuzin, N.I. (1968) The petrology of grospydite xenoliths from the Zagadochnaya Kimberlite pipe in Yakutia. Journal of Petrology, 9, 253–280.

Sobolev, N.V., Schertl, H.-P., and Burchard, M. (2001) An unusual pyrope-grossular garnet and its paragenesis from diamondiferous carbonate-silicate rocks of the Kokchetav Massif, Kazakhstan. Doklady Earth Sciences, 380, 791–794.

Ulbrich, H.H. and Waldbaum, D.R. (1976) Structural and other contributions to the third-law entropies of silicates. Geochimica Cosmochimica Acta, 40, 1–24.

Vinograd, V.L. (2001) Configurational entropy of binary silicate solid solutions. In C.A. Geiger, Ed., European Notes in Mineralogy—Solid solutions in silicate and oxide systems, 3, 303–346.

Vinograd, V.L., Sluiter, M.H.F., Winkler, B., Putnis, A., Halenius, U., Gale, J.D., and Becker, U. (2004) Thermodynamics of mixing and ordering in pyrope-grossular solid solution. Mineralogical Magazine, 68, 101–121.

Wang, L., Essene, E.J., and Zhang, Y. (2000) Direct observation of immiscibility in pyrope-almandine-grossular garnet. American Mineralogist, 85, 41–46.

MANUSCRIPT RECEIVED JUNE 10, 2005
MANUSCRIPT ACCEPTED JANUARY 20, 2006
MANUSCRIPT HANDLED BY ANDREAS LUTTGE